

## HIGH-EFFICIENCY MICROTURBINE TECHNOLOGY

F. David Doty, Brian L. Miller, Greg S. Hosford  
Doty Scientific, Inc.

David Gordon Wilson  
Massachusetts Institute of Technology

Wu Huanbo and John Dewey Jones  
Simon Fraser University

### ABSTRACT

Most microturbines have low efficiency, due to low Reynolds numbers and large relative losses from high clearance-to-flow-passage dimension ratios. We have demonstrated a single-stage, radial-inflow, 21-W air micro-turbine with an isentropic efficiency of over 40% at room temperature.

The turbine is made from low-cost materials by a straightforward process, which is readily adaptable to large-scale production on a high-precision 4-axis CNC lathe. It employs hydrostatic gas bearings of our own design. The gas bearing design eliminates whirl instabilities for bearing surfaces up to the working fluid's sonic velocity.

Applications of the technology are discussed. Design philosophy and basic calculations for the turbine are presented. Experimental testing of the turbine is described, and the results compared with the predictions of a simple computer model.

### INTRODUCTION

Anyone who has had dental work done has been in intimate contact with a microturbine spinning at 1 to 10 kHz (60,000 to 600,000 rpm). There is no particular reason why turbines in dental drills should be efficient, and in fact they are not - a typical efficiency figure is 5-10%. For some applications, though, small dimensions and high efficiency are both desirable - Reverse Brayton cycle refrigeration in space-based systems, for example, or high speed sample spinners for spectral line narrowing in nuclear magnetic resonance (NMR) spectroscopy of solid samples.

On the macroscopic scale - for a 100-MW turbine, for example - it is not difficult to achieve turbine polytropic efficiencies above

93% [10]. Why does it become so much more difficult to achieve comparable levels when the design is scaled down?

The two factors chiefly responsible are the greater importance of viscosity in small ducts, and the difficulty of achieving close tolerances. If the reader wishes to get a scaled-up view of these difficulties, imagine using a hammer and chisel to carve out a turbine that will extract power from a fast-flowing jet of molasses.

### INTENDED MICROTURBINE APPLICATIONS

#### NMR Sample Spinners

Although seldom encountered outside the discipline of physical chemistry, the widely used NMR analytical technique of "Magic Angle Spinning" uses microturbines to rotate samples at rates exceeding 20 kHz. This technique, used to determine molecular structures, depends critically on being able to rotate small samples with surface speeds near the sonic velocity at various angles with respect to a magnetic field [1],[4],[11]. The recent interest in spinning larger samples at higher speeds for improved sensitivity requires higher efficiencies and improved gas bearings. This need served as our initial motivation for the present work, as this technique is a critical component of an industry segment that does \$100M worth of business annually.

Figure 1 shows an axial cross section of a sample spinner design that has been used for several years to spin 5-mm-diameter silicon nitride sample containers at rates exceeding 17 kHz (over 1,000,000 rpm) using room temperature nitrogen for the turbine and gas bearing. The air bearing friction amounts to nearly 10 W at these speeds. These simple, self-centering impulse turbines achieved a meager 5 to 8% efficiency at about 5 W each.

IECEC-91 p. 436-442

The low efficiency of these impulse microturbines with simple buckets requires relatively high nitrogen gas consumption. The NMR experiment often needs to be performed at elevated temperatures to observe structural and phase changes as a function of temperature. In the space confines within the bore of a superconducting magnet, this presents gas heating and subsequent cooling problems that generally scale as the volume of gas consumption. Hence, the reduction in gas consumption that is afforded by improved efficiency is quite beneficial.

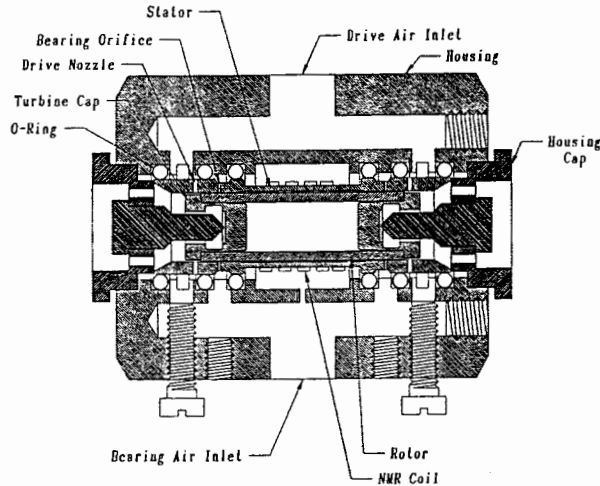


Figure 1. A 17-kHz, 5-mm NMR sample spinner. The zirconia or silicon nitride rotor cylinder (sample container) is driven by plastic (polyimide) impulse turbine caps at opposite ends. Air jets from drive nozzles impinging on the buckets produce the desired spinning. Rotor surface speeds are typically 30-70% of the speed of sound. A manifold inside the zirconia housing distributes pressurized nitrogen to the bearing orifices and the drive nozzles. The receiver/transmitter NMR coil is wound around the stator. The nitrogen exhausts through holes in the housing cap.

#### Cryocooling

Study of the available cryogenic technologies indicates that one of the most promising means of cryorefrigeration is the reverse Brayton cycle, or RBC. The RBC has often been used at cooling powers above 1 kW because it allows high efficiency over a wide range of load conditions and permits very compact expanders. Also, the expanders and compressors can be designed for virtually zero vibration and noise. These appealing

features have repeatedly lured researchers to attempt to produce small RBC cryocoolers, but the dream has always been beyond their grasp. The conclusion has repeatedly been that the RBC cannot be scaled down below several hundred watts at 70 K, or below several tens of watts at 6 K [3], [13]. We hope now to be able to scale down another order of magnitude for applications in aerospace detector cooling and Magnetic Resonance Imaging (MRI) magnet cooling [1]. Part of our optimism in this application is based on the progress we have demonstrated in the other critical component of the RBC cryocooler - the recuperator [9].

The Figure of Merit (FOM) of small Gifford-McMahon cryocoolers is typically less than 0.08, i.e., they operate at less than 8% of the Carnot efficiency. Large Collins-cycle liquefaction systems for nitrogen have a typical FOM of 0.2, while for helium this figure falls below 0.15. By contrast, the theoretical Figure of Merit for the Reverse Brayton Cycle as the pressure ratio approaches unity is equal to the Carnot limit. We believe practical RBC cryocoolers can achieve an FOM of 0.3, while large systems might exceed 0.6. The major limitation in small systems is the expander turbine efficiency, while the limitation in large systems is the recuperator cost.

The most convincing argument against the RBC is usually the cost of its cryogenic turbine expander, since the J-T cryocooler needs only a simple orifice and the piston displacers of the Gifford-McMahon (and Stirling) cycle are well-developed. Available turbine expanders are often priced near \$100,000 each in small-scale (20 units/year) production. On the basis of the work described below, we believe it should now be possible to build high-efficiency cryogenic expanders from several watts to hundreds of kilowatts at very low cost. The small expander cost is offset many times over by the 30% to 80% reduction in recuperator cost and some reduction in the compressor cost afforded by the RBC.

#### Heat Pumps

The reverse Brayton cycle can also be used as the basis for residential and commercial HVAC heat pumps, and, as in the cryogenic application, it will permit higher coefficients of performance than available with conventional designs. Although such heat pumps will cost more to produce than current commercial units, the reduced operating costs over the

life of the heat pump will result in substantial savings. Furthermore, RBC heat pumps use environmentally safe working fluids, such as helium and nitrogen, instead of the chlorofluorocarbons used in current systems.

### MICROTURBINE DESIGN

Radial-axial mixed inflow turbines are widely used in the power range of 0.5-500 kW with Reynolds numbers of 20,000-1,000,000, but they have usually been considered impractical at lower powers. However, somewhat smaller versions may be found in cryogenics, where the high gas densities and low viscosities permit Reynolds numbers above 20,000 with sub-millimeter blade dimensions.

Prior approaches to efficient microturbine design have used essentially isotropic reductions of designs that have worked well in the several kilowatt range - mixed flow, radial-axial. The problem with this approach is that it is virtually impossible to reduce the diameter below several mm or rotational rates become too high for available bearings, shafts, and loads. The approach which we find preferable is to use a purely radial inflow design that allows the axial blade dimension to be reduced to a small fraction of a millimeter while maintaining turbine diameters above several millimeters [7].

High-efficiency single-stage turbines must operate with tip speeds at nominally half the speed of sound or higher. Low power levels require minuscule nozzle areas. The radial inflow geometry, as illustrated in Figures 2 and 3, allows extremely small flow areas at high tip speeds without excessive rotational frequencies when the axial blade length is made extremely short at the perimeter. In the purely radial inflow turbine, the

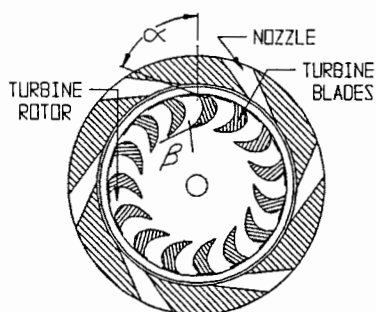


Figure 2. End view of a radial inflow microturbine.

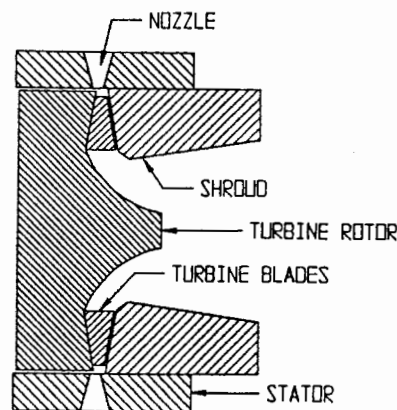


Figure 3. Axial cross section of a radial inflow microturbine.

airfoil blades protrude axially from a rotating support plate. Nozzles admit high-velocity gas inward from the perimeter at the proper entrance angle. The gas flows radially inward over the blades with entrance angle  $\alpha$  and exits radially inward off the trailing edge of the blades at an exit angle  $\beta$  in the negative direction. The gas flow is turned to exhaust axially after it passes the inner diameter of the blades. The blade length need not be constant in the radial or axial direction to classify as a purely radial inflow turbine, but the gases are not allowed to exhaust over the blades with a substantial axial component. The radial blade dimension needs to be less than half of the drive plate radius to allow higher exhaust gas velocity without swirl and so that the flow can be turned axially after exiting the blades.

The radial inflow blade geometry permits high efficiency with greatly simplified manufacturing of hard ceramics and composites owing to the absence of compound angles and their resulting concave contours of small radii at the base of the blades. The blade surfaces are generally parallel to the axis. The blade end geometry also simplifies the requirement of making the axial-end leakage past the blades very small by simplifying the end shroud geometry. Blade axial-end clearance ideally should be several percent of the axial blade length. It will typically be under 10% of the axial blade length in microturbines. Clearances twice that large will also perform satisfactorily for low reaction designs. Axial blade length at the

perimeter is typically 0.2-0.5 mm. At the smallest sizes (2.2 mm outside diameter) we use only eight blades, but 30-40 blades are preferable above 10-mm diameter. Continuously inwardly decreasing cross-sectional-flow-area passages and sharp trailing blade edges are required for minimum flow separation and high efficiency.

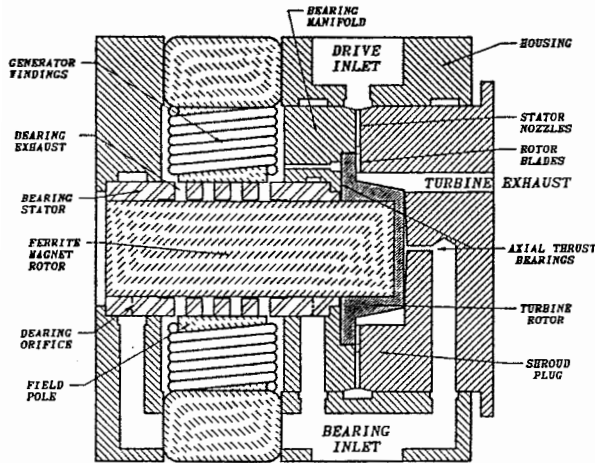


Figure 4. Axial section of the 10-mm micro-turbine-generator.

#### The Microturbine Test Apparatus

An axial cross-sectional view of the 10-mm, 20-W turbine test apparatus is shown in Figure 4 at approximately three times actual size. (Most of the parts are substantially symmetric about the axis of the ferrite magnet.) The polyetherketone (PEK) turbine rotor is pressed over the end of a strontium ferrite rod, 5 mm diameter x 15 mm long. The rod was cut and ground from oriented bulk material in such a way that the preferred magnetization axis lay along a diameter. This anisotropic rod was then permanently magnetized along the preferred diameter and served as the rotor in a dipolar generator. We opted to use a generator load rather than the more common compressor loading technique because we believe the generator simplifies contamination and control problems in cryocooler expander applications.

The ferrite rotor magnet also serves as the radial gas bearing journal. Hence, extreme precision ( $\pm 3 \mu\text{m}$ ) is required on its diameter, but length is practically irrelevant. (The anisotropy of the material complicates the procedure for obtaining the roundness specification, as the roundness is slightly affected by the magnetization state - i.e., the material is somewhat magnetostrictive.) The critical rotor blade axial-end clearance is controlled by axial thrust gas bearings on opposite sides of the short rotor disk and several mating parts. This feature is very significant for ease of machining and successful operation over a wide range of temperatures.

The gas bearing stator surrounding the rod was machined from Macor, a machinable ceramic-glass by Corning. Pressurized gas is admitted through a circle of bearing orifices near each end of the ferrite rod to establish the radial gas bearing. Gas from a single axial hole in the shroud plug establishes the thrust bearing in one direction. An opposing thrust bearing is established by the radial bearing gas which exhausts over the opposite face of the turbine rotor. The nozzles are machined into the PEK shroud plug. The nozzles in the shroud plug seal against a surface of a PEK bearing manifold that includes several channels for proper operation of a radial gas bearing and a thrust bearing. A two-pole, manganese-zinc ferrite core supports the generator field windings.

The PEK housing supports the Macor bearing stator, PEK bearing manifold, PEK shroud plug, and generator field, and it distributes the pressurized gas to the bearings and nozzles. The entire expander with generator includes a total of eleven parts (five of which comprise the generator field and copper windings) that are rather easily manufactured by conventional methods. We would expect to substitute partially stabilized zirconia (PZT) for Macor in production units, and perhaps carbon-fiber-reinforced PEK would be used for the turbine rotor. High pressure injection molding techniques could be used for manufacture of the plastic parts in larger volume production.

#### Gas Bearing Whirl Control

The above discussion belies the difficulties usually encountered in producing gas bearings with adequate stability. Hydrostatic gas bearings are known to be fraught with whirl instabilities [18]. When the rotor is dis-

placed slightly from concentricity within the stator, the shaft rotation pumps the gas to a higher mean pressure on the converging side of the bearing clearance space compared to the diverging side. This gives rise to a whirl force perpendicular to the hydrostatic restoring force. The mean rotational speed of the air mass between the rotor and stator is approximately half the rotational speed of the rotor surface. As a result, at rotational frequencies somewhat below half of the static resonant frequencies, as calculated from bearing stiffness and rotor moments, the rotor will whirl, that is, the rotor's center will execute a small-radius orbit.

A novel, general solution to this problem has been found. One feature of our solution is that it allows greater clearance by a factor of four than is typically found in gas hydrodynamic (e.g., foil, herringbone grooved, tilting pad, etc.) bearings [17]. Hence, reliability and manufacturability are greatly enhanced and friction is greatly reduced. Gas consumption is increased, but this is seldom a significant drawback in either expander turbines or in electric-motor-driven centrifugal or turbine compressors, where an abundant source of pressurized gas is available. Stiffness is much higher than can be achieved in foil-type hydrodynamic bearings, owing to the compliance of the foils, and whirl is inhibited even for transonic bearing surface speeds.

The optimum radial clearance  $r_c$  (in mm) for our anti-whirl hydrostatic gas bearing is found to be given by the following:

$$r_c = k T^{.55} r^{.33} \quad (1)$$

where  $T$  is the temperature in kelvins,  $r$  is the rotor radius in mm, and  $k$  has numeric value between 0.0007 and 0.0009 for nitrogen (with units,  $K^{-.55} \text{ mm}^{.67}$ ). For helium,  $k$  has numeric value between 0.0011 and 0.0015. Optimum values for hydrogen are similar to those for helium, and optimum values for heavy gas mixtures are similar to those for nitrogen.

Bearing gas mass flow with the journal (rotor) in place lies in the range of 50-90% of the bearing mass flow with the journal removed for similar applied pressures. Optimum flow ratios are about 35% for prior designs. Other key features of our novel stabilization technique will be presented in a subsequent paper [8].

## The Computer Micro-turbine Model

We have devised a prototype computer model of the microturbine, which we will develop to the point where it can accurately predict efficiency, power, mass flow rates and temperature ratios and determine optimum blade angles.

The first part of the model involves a careful calculation of the properties of the working fluid. Notable improvements in system performance can sometimes be obtained by using a suitably chosen mixture of gases as the working fluid [5]. We can deal with mixtures involving up to fifteen non-reacting gases in arbitrary ratios.

Rather than attempting a full three-dimensional model of the gas flows within the turbine, we treat all flows as one-dimensional. To find the mass flow rate through the turbine, we estimate an initial value for the ratio of pressure drops across the stator and rotor. From the initial estimate of pressure drop across the stator, we calculate the mass flow rate, based on an empirically determined discharge coefficient for the micro-nozzles. Using this mass flow rate, we calculate the pressure drop across the rotor, and hence obtain a new value for the ratio of pressure drops; we iterate on this calculation until convergence is obtained.

Each time through the loop, we also calculate ideal power and estimate various losses, treating them as decoupled and independently calculable: bearing losses, nozzle flow shear loss, nozzle exit turbulence, the rotor entrance loss, the rotor passage turbulence loss, the rotor blade flow shear loss, power loss due to blade blowby, the effects of laminar boundary layer at the blade end, radial and rotational exhaust power losses.

## Experimental Work

Before the model can be used as a guide to design, it must be checked against experiment. Table 1 gives some of the key parameters for one of our microturbines. Unfortunately, while it is easy to measure the overall turbine power and efficiency, it is difficult to resolve the measured loss into the separate factors represented in the program. Partial validation can be achieved by plotting efficiency versus speed for different load conditions: some loss factors vary as the mass flow rate, some as a higher power of flow rate.

Table 1. Microturbine parameters

Turbine Tip O.D.	14 mm
Air bearing O.D.	7 mm
Number of nozzles	12
Nozzle throat width	0.42 mm
Number of rotor blades	36
Blade height	0.38 mm
Blade tip clearance	30 $\mu$ m
Typical reaction ratio	30 %
Typical blade Reynolds number	4200

Figure 5 gives a diagram of the experimental set-up. The temperature differential between T1 and T2 was measured using chromel-alumel thermocouples with a digital read-out. In making this measurement, care was needed to avoid inaccuracy due to heat conduction along the thermocouple wires.

To start the experiment, nitrogen was supplied to the air bearing, and then to the turbine inlet. 'Cogging' within the generator caused sufficient initial resistance to rotation that it was necessary to administer a brief burst of 60 Hz current from a low voltage transformer to the coil terminals to start the rotor spinning.

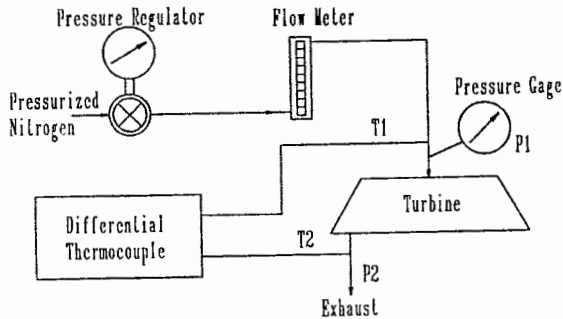


Figure 5. Microturbine test setup.

A variable resistive load, R, was put across the terminals. The frequency and amplitude of the voltage across R were measured using an oscilloscope. The total pressure at point P1 measured using an oil-damped pressure gauge. The volumetric flow rates to the turbine and the bearing were measured using Dwyer floating-ball flowmeters. The indicated flow rate was corrected according to the manufacturer's instructions - proportional to the square root of the absolute density. The turbine exhausted to atmosphere.

The power output was calculated in two ways: (1) from the temperature and mass flow measurements, via the formula

$$P_0 = c_p G(T_1 - T_2) \quad (2)$$

where  $c_p$  is the specific heat and G is the mass flow rate; (2) from the measured voltage across the resistance. The second calculation would be expected to give a lower value than the first, due to the efficiency of the generator being less than 100% and due to the bearing friction losses, which were calculated by the computer model to be typically in the range of 1 to 6 W. These losses were separated by comparing experimental losses with and without the generator stator in place. The calculated bearing losses were found to agree with the experimental values within the limits of our ability to measure clearances -  $\pm 10\%$ . Hysteresis losses for the unloaded (open circuit) generator were determined to be approximately 5 W ( $\pm 1$  W) at 4 kHz and linear with frequency. This resulted in generator efficiency being much less than hoped for. A quadrupolar design has been shown to be much better in this regard and will be used in future work. Generator efficiency was further degraded several percent by resistive losses in the windings. The remaining discrepancies in the data in Table 2 are believed due primarily to flow measurement calibration errors, but additional bearing and generator losses are not ruled out. A small, systematic error arises from ignoring the Joule-Thompson effect.

Table 2 shows the turbine power output and gross efficiency as a function of speed for several load conditions.

Table 2. Microturbine output measurements.

$P_1$ kPa	G g/s	f Hz	$\eta_T$ %	$P_{ST}$ W	$P_{BL}$ W	$P_E$ W
140	.67	3836	36	10.7	4.7	0
140	.68	2893	37	10.9	2.7	3.7
140	.69	2367	36	10.9	1.8	5.2
200	.85	4200	41	20.8	5.7	5.2
200	.86	3660	41	20.8	4.3	7.5
200	.87	3280	40	20.3	3.5	8.7
240	1.02	4060	43	32.5	5.4	14.5

In the above,  $p_1$  is turbine inlet pressure, G is mass flow rate, f is the rotational frequency,  $\eta_T$  is theoretical efficiency from temperature drop,  $P_{ST}$  is calculated shaft power,  $P_{BL}$  is bearing power loss, and  $P_E$  is measured electrical output power.

A tentative experimental conclusion is that efficiency of our micro-nozzles is much lower than we predict from our CFD-based estimates of boundary layer thickness and mixing of these flows. While we expected efficiencies above 0.9 for subsonic nozzles with throat diameter 0.3 mm, preliminary indications are that the over half of the total losses occur in the nozzles and rotor inlet plenum. A surprising experimental conclusion is that the effects of blade entrance and exit angles are relatively minor. Another surprise was to find best efficiency when the clearance between the nozzles and rotor blades was about twice the nozzle flow width. Finally, based on several measurements of static pressure in the plenum between the nozzle exhaust and the rotor blade entrance, we appear to be achieving a much lower reaction ratio than expected, which probably indicates greater blowby than expected. However, we must emphasize the preliminary nature of these conclusions.

### CONCLUSIONS

We have demonstrated much higher gross efficiency - over 40% - than any previous work to our knowledge for air powered turbine-generators below 20 W operating at room temperature with inlet pressure below 0.24 MPa and outlet pressure 0.1 MPa. The design is easily manufacturable by conventional methods, and we are at the moment scaling it down for a 3-W version. Our attempts to develop a computer model useful for further optimization have achieved only limited success thus far, but preliminary indications are that substantial improvements in efficiency can be expected for our microturbines at cryogenic temperatures owing especially to the reduced viscosity and sonic velocity at low temperatures and the attendant increase in Reynolds number for a given power level.

### REFERENCES

- [1] Ackermann, R. A. (1990) "Cryorefrigerator Evaluation for Future Magnetic Resonant Imaging Applications", International Cryocooler Conference 6, Plymouth, MA.
- [2] Andrew, E. et al (1969) J. Magn. Reson. 1.
- [3] Barron, R. F. (1985) Cryogenic Systems. Monographs on Cryogenics 3, 2nd ed., Oxford, NY.
- [4] Doty, F. D., and Ellis, P. D. (1981) "Design of High Speed Cylindrical NMR Sample Spinners," Rev. Sci. Instrum., 52 (12).
- [5] Doty, F. D. and Jones, J. D. (1990a) Proceedings, IECEC-90, "A New Look at the Closed Brayton Cycle".
- [6] Doty, F. D. and Jones, J. D. (1990b) "The Micro-Tube Strip Heat Exchanger", J. Heat Transfer Engr. in press.
- [7] Doty, F. D., Spitzmesser, J. B., and Wilson, D. G. (1991a) "High Temperature NMR Sample Spinner", patent pending.
- [8] Doty, F. D., Hacker, L. G., and Spitzmesser, J. B. (1991b) "Supersonic Sample Spinner", patent pending.
- [9] Jones, J. D. and Doty, F. D. (1990) "A Laminar Flow Heat Exchanger", Proceedings, IECEC-90.
- [10] Lidsky, L. M. (1988) "A Direct-Cycle Gas Turbine Power Plant for Near-Term Applications: MGR-GT," Proc. Tenth International HTGR Conference, San Diego, CA.
- [11] Pines, A. and Samoson, A. (1990) "Probe for High Resolution NMR with Sample Reorientation", U. S. Patent 4,899,111.
- [12] Voth, R. O., Norton, M. T., and Wilson, W. A. (1965) "A Cold-Moderator Refrigerator Incorporating a High-Speed Turbine Expander", Adv. Cry. Engr. 11.
- [13] Sixsmith, H., Valenzuela, J., Swift, W. L. (1987) "Small Turbo-Brayton Cryocoolers", Adv. Cry. Engr. 33.
- [14] Shapiro, A. H. (1953), Compressible Fluid Flow, Vol. I, Wiley, NY.
- [15] Tilliette, Z. P. (1987) J. Engr. for Gas Tur. and Power, 109, 92.
- [16] Wilson, D. G. (1984) The Design of High Efficiency Turbomachinery and Gas Turbines, MIT Press, Cambridge, Mass.
- [17] Yang, J. L., and Munday, A. M. (1982) "A Grooved Self-Acting Bearing for use in Cryogenic Expansion Turbines," Cryo. Processes and Equipment, Vol. 79.
- [18] Yang, K. L. et al (1990) "Application and Test of Miniature Gas Bearing Expansion Turbines," Adv. Cry. Engr., Vol 35.